Experiment and analysis for an improved design of the inlet and nozzle in Tesla disc turbines

A Guha and B Smiley

The online version of this article can be found at:
http://pia.sagepub.com/content/224/2/261

Published by:

$SAGE

http://www.sagepublications.com

On behalf of:

Institution of MECHANICAL ENGINEERS

Institution of Mechanical Engineers

Experiment and analysis for an improved design of the inlet and nozzle in Tesla disc turbines

A Guha[*,‡] and **B Smiley**
Aerospace Engineering Department, University of Bristol, Bristol, UK

Abstract: In this article, the performance of the inlet to a Tesla disc turbine has been studied. The losses in the inlet and nozzle are known to be a major reason why the overall efficiency of disc turbines is not high. A new nozzle utilizing a plenum chamber inlet has been designed and tested here. Experiments have demonstrated less than 1 per cent loss in total pressure in the new design compared to losses in the range 13–34 per cent for the original nozzle and inlet. Other than the dramatic improvement in loss reduction, the new plenum-integrated nozzle achieves a considerable enhancement in the uniformity of the jet. This has been demonstrated here both by experimental traverses of Pitot tubes as well as computational fluid dynamics studies. The greater uniformity of the jet means that a single Pitot measurement approximately positioned at the centre of the jet would record a value close to the true centre-line total pressure, and that calculations based on centre-line values of total pressure would give, to a good accuracy, the average loss coefficient of the nozzle–inlet assembly. The uniformity of the jet also means that all disc passages would receive uniform inlet conditions; this should improve the performance of the rotor thereby further enhancing the overall efficiency of the Tesla turbine.

Keywords: Tesla turbine, efficiency, power, nozzle, rotor, jet, pitot traverse, computational fluid dynamics

1 INTRODUCTION

In this article, we report design improvements to a Tesla disc turbine and an experimental and theoretical investigation into its operating characteristics. It has previously been recognized [1–3] that the performance of the nozzle and the inlet is a limiting factor for the overall efficiency of such turbines. The detailed flow features of an existing nozzle–inlet assembly are analysed here and the sources of major losses are identified. This then led to an improved design. Experimental and computational results show that the performance of the new nozzle–inlet assembly is significantly improved. This would have a substantial

impact on the overall performance of Tesla disc turbines. In reference [2], Rice writes: 'In general, it has been found that the efficiency of rotor can be very high, at least equal to that achieved by conventional rotors. But it has proved very difficult to achieve efficient nozzles in the case of turbines. [...] As a result, only modest machine efficiencies have been demonstrated.' This article therefore addresses and solves a major issue in the design of Tesla disc turbines that seems to have seriously affected their development for over 50 years.

1.1 Operating principle

The Tesla disc turbine is a bladeless turbine invented by Nikola Tesla in 1913 [4, 5]. Fluid is injected through a nozzle nearly tangentially onto an array of co-axial flat discs. As the fluid moves through the gaps between the discs shear stresses arise due to the difference in tangential velocities of the discs and the fluid. The shear stresses acting over the surface area of the discs give

*Corresponding author: Aerospace Engineering Department, University of Bristol, University Walk, Bristol BS8 1TR, UK.
email: A.Guha@bristol.ac.uk; guha.a@rediffmail.com
[‡]*Now at: Mechanical Engineering Department, Indian Institute of Technology, Kharagpur 721302, India.*

rise to a torque and allow work transfer from the fluid to the rotor. The fluid exits the rotor through holes in the discs near the shaft with a throughflow velocity in the axial direction.

1.2 Perspectives of development in Tesla turbines

The disc turbine showed early promise. Initially Tesla, with the help of *Allis Chalmers Company* built a turbine with a power output of 500 kW [**6**]. After testing, the discs were inspected and found to have been stretched by radial stresses resulting from the high angular velocity of the turbine. It is likely that the stretching was due to the choice of steel used which had a low yield point [**6**]. This setback and lack of funds caused *Allis Chalmers Company* to stop development of the Tesla turbine and focus instead on the *Curtis* and *Parsons* type of Impulse and Impulse-Reaction machines [**6**]. From the 1950s onwards there was a resurgence of interest in the Tesla turbine and a number of disc turbines were built and tested [**1**, **3**, **7**–**9**]. In these experimental investigations, the efficiencies demonstrated by the Tesla turbine have been in the range 14.6–35.5 per cent [**10**], which is low compared to modern day gas turbines which has an efficiency of around 90 per cent [**11**].

Even though the efficiency of the Tesla turbine is low compared to conventional turbomachinery it may find application in special areas where it has an advantage over bladed turbines. The first advantage is the simplicity of design and manufacture. It is also relatively inexpensive. The turbine could be useful in situations where very viscous or non-Newtonian working fluids are used, or with non-conventional fuels such as biomass. It is believed that Tesla turbines can cope better with particle-laden two-phase flows because of the self-cleaning nature of the discs (references [**12**] to [**16**] describe the general aspects of two-phase flows).

Other than the nozzle–inlet assembly, losses occur in the disc rotor itself. Analytical investigations have been published with the aim of predicting the maximum isentropic efficiency of the disc rotor. A study conducted by Lawn and Rice [**17**] concluded that the maximum theoretical efficiency of the disc rotor was 81 per cent. This agrees with the findings of Allen [**18**], who predicted possible efficiencies exceeding 80 per cent. More recently, a paper by Rice [**2**] predicts that the maximum efficiency of the rotor could exceed 95 per cent. The new design described in this article paves the way for the efficiency of the rotor to be determined experimentally for the first time.

The Tesla turbine, to date, has not been used commercially. This is mainly due to the low turbine efficiencies demonstrated. Since the gas turbine cycle has a poor work ratio (thereby the component efficiencies having a strong impact on the cycle efficiency), the efficiency of the Tesla turbine has to be improved substantially over its current values for its use in place of the conventional turbines even in niche application areas.

1.3 Difference between experimental and theoretical efficiency

It can be seen that there is a large difference between the theoretical maximum efficiency of the disc turbine and the efficiencies demonstrated experimentally. In his paper of 2003 [**2**], Rice states that there is little to no literature devoted to the flows that cause the main losses in the Tesla turbine.

Investigators have focused their attention on the disc rotor and little attention has been paid to other key components in the turbine such as the nozzle and the exhaust. As a result, no attempt has been made to measure losses in these components individually and apparently no research has gone into improving their design.

The discrepancy between theoretical and experimentally demonstrated efficiencies could also be due to the difficulty faced by investigators when trying to optimize the turbine. There are many parameters which can be changed and there is extensive cross-coupling between them. After the success of Whittle and von Ohain, the gas turbine became the centre point of research and development, and the understanding of its performance and optimization has reached quite a mature stage [**11**, **19**–**23**]. The understanding of the performance of Tesla turbines is not nearly as thorough. This has resulted in lower than optimum efficiencies.

1.4 The scope of the present study

In this study, a detailed investigation into the inlet and nozzle of the Tesla turbine is conducted. Rice [**2**] states that the efficiency of the disc rotor can be very high, at least equal to that achieved by conventional rotors, but that it has proved very difficult to achieve efficient nozzles in the case of Tesla turbines. Rice [**2**] goes on to say that there are inherent losses as the fluid enters the rotor because the nozzles in Tesla turbines are necessarily long and inefficient.

In an earlier phase of this project a Tesla turbine was designed, built, and tested [**3**]. A thorough analysis of the turbine is presented in reference [**3**]. The inlet and nozzle of this turbine were designed on the basis of knowledge reported in the existing literature and therefore suffer from similar limitations. The inlet was assembled from off-the-shelf pneumatic parts and was long and complex. However, the inlet incorporated an innovation in that it allowed nozzles with different geometries to be interchanged without any modification of the turbine casing being necessary.

The maximum efficiency of this turbine was approximately 25 per cent [3], which is similar to the efficiencies found in the literature. A detailed study into the performance of the inlet presented in this article, which incorporates experimental and computational fluid dynamics (CFD) analysis, showed that the nozzle and inlet were responsible for losses in stagnation pressure up to 35 per cent. This confirms that Rice [2] was correct to suggest that the nozzle and inlet were critical components in the Tesla turbine.

A new inlet was therefore designed, manufactured and tested. The findings are reported in this article. The new design retained the flexibility of the test rig described in reference [3], but allowed losses in stagnation pressure due to the nozzle and inlet to be reduced to below 1 per cent. This could be significant for achieving commercial viability of the Tesla turbine.

Section 2 outlines methods for calculation of the performance of the turbine nozzle and inlet, and applies them to existing designs to assess and identify problem areas. Section 3 then describes the rationale for the design of a new nozzle and new inlet based on the knowledge gleaned from the calculations of section 2. Section 4 describes the experimental set-up used for the present study, and compares the experimental results for the performance of the new designs with that for the existing designs of the turbine nozzle and inlet. Appendix 2 describes a CFD analysis of various nozzle–inlet assemblies. Appendix 3 presents analytical formulation for designing and analysing plenum chambers, together with the numerical scheme to solve the equations.

2 METHOD OF ANALYSIS FOR TURBINE NOZZLE AND INLET

2.1 Description of turbine inlet and nozzle

In this section, the turbine that was built in an earlier phase of this project [3] is described with particular attention paid to the nozzle and inlet. Methods are presented which allow total pressure losses in an arbitrary turbine inlet to be determined. Using these methods an estimate for the loss coefficient in the current turbine inlet and nozzle is calculated.

2.1.1 Description of turbine

The main features of the turbine were designed according to experience noted in references [2], [5], [6], [8], and [9]. The disc diameter is 92 mm (3.6 in), the thickness of each disc is 0.9 mm, and the rotor-to-housing diametrical clearance is 0.3 mm. An overall view of the turbine can be seen in Fig. 1. The discs have a single central outlet port, since this configuration was found to be more efficient by Davydov and Sherstyuk [9] and Rice [2]. In order to accommodate the

outlet of the fluid, the shaft is supported as a cantilever by means of bearings inside the base-plate (Fig. 1(d)).

2.1.2 Description of nozzle

The overall design of the turbine is very flexible allowing parameters to be varied in order that their effect on the performance of the turbine can be measured. It is possible to change the number of discs, disc spacing, and geometry of the nozzle without changing the base-plate or housing. The geometry of the nozzle can be changed using an interchangeable nozzle insert. As a design compromise it was necessary that the nozzle incorporated a 90° bend just before the exit plane. The nozzle insert can be seen in its position in Fig. 1(c). The nozzle outlet area is rectangular. In this article, the major dimension of the nozzle outlet is called height and the minor dimension is called width. The height of the slot-shaped nozzle can be adapted to the variable axial extent of the rotor (which depends on the number of discs used) by using inserts with the shape of the nozzle channel, this is so that the unused area of the nozzle can be blocked and the jet can be directed more efficiently to the rotor avoiding major leakages. (However, it is suspected that the inserts may not have blocked the intended area completely, allowing a small amount of leakage.)

2.1.3 Description of inlet

The inlet and nozzle for the turbine are shown in Figs 1(b) and (c) respectively. The working fluid is delivered by 8 mm hosing to a series of off-the-shelf pneumatic fittings. First, there is a push-on-hose fitting which attaches via an adapter to an elbow which channels the flow into the base-plate. The elbow contains a static pressure tapping and a total pressure probe. The duct drilled into the base-plate aligns with the hole in the nozzle insert allowing the fluid to enter the nozzle. The seal between the two sections is maintained by an O-ring.

2.1.4 Definition of nozzle and inlet

For the purposes of this article, the turbine inlet is defined as the section of duct from the start of the elbow fitting until the beginning of the nozzle insert. The nozzle is defined as the fluid path starting from the 6 mm entrance to the nozzle insert up until the point at which the fluid exits the nozzle.

2.2 Analytical tools for predicting stagnation pressure drop along ducts

Empirical methods for predicting total pressure losses caused by the nozzle and inlet were used to estimate the potential magnitude of losses in the inlet and provide physical insight. It is suggested in Crane [24]
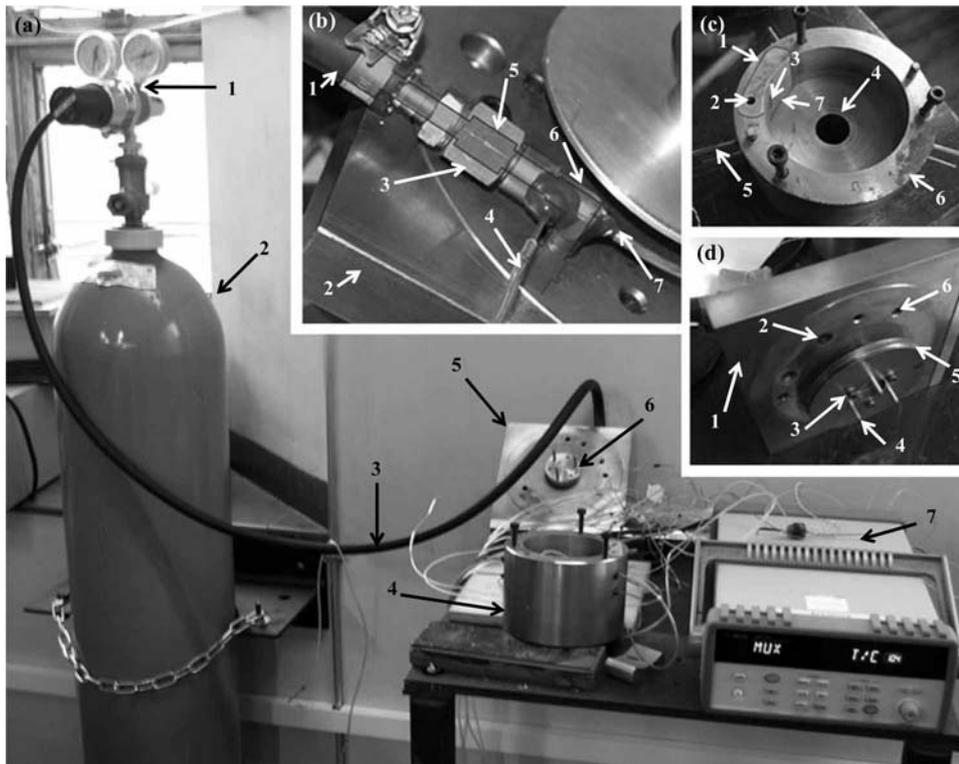
Fig. 1 (a) Overall view of the test rig and turbine. Keys: (1) pressure regulator, (2) air cylinder, (3) supply line, (4) turbine housing, (5) base-plate, (6) spindle, and (7) data logger. (b) Detailed view of turbine inlet. Keys: (1) supply line, (2) base-plate, (3) pneumatic fittings, (4) static pressure tapping, (5) superimposed image of internal diameter changes of inlet, (6) elbow fitting, and (7) Pitot probe. (c) Detailed view of turbine housing. Keys: (1) nozzle insert, (2) entrance to nozzle, (3) nozzle exit, (4) exhaust hole, (5) static pressure tappings (one of the nine labelled), (6) turbine housing, and (7) potential fluid leak path. (d) Detailed view of turbine rotor. Keys: (1) base-plate, (2) interface between the inlet and the entrance to the nozzle insert, (3) bolts holding the discs (one of the three labelled), (4) locating pins (one of the three labelled), (5) discs, and (6) bolt holes connecting base-plate to housing (one of five labelled)

that losses in ducts are caused by four main mechanisms.

1. Friction against the walls of the duct.
2. Viscous eddies caused by abrupt or gradual changes in duct cross-sectional area.
3. Pressure gradients and secondary flows caused by changes in the duct direction.
4. Faulty seals leading to leakage of fluid to the atmosphere.

Methods for predicting losses caused by these mechanisms are examined in turn.

2.2.1 Friction against the walls

In any duct system, mechanical energy is lost through viscous interaction between the fluid and the walls. The relationship between wall friction and pressure

drop can be expressed using Darcy's equation [**24**, **25**]

$$\Delta p_\mathrm{f} = \frac{1}{2} k_\mathrm{f} \rho u^2 \tag{1}$$

$$k_\mathrm{f} = F \frac{l}{d} \tag{2}$$

2.2.2 Changes in duct cross-sectional area

When an abrupt enlargement in duct cross section occurs, the flow cannot follow the contour of the duct causing separation. Turbulent eddies form in the region of separation causing energy to be dissipated in the form of heat. An expression for the pressure loss coefficient can be found analytically by combining the continuity, steady flow momentum and incompressible energy equations [**25**]

$$\Delta p_\mathrm{e} = \frac{1}{2} k_\mathrm{e} \rho u_\mathrm{i}^2 \tag{3}$$

$$k_\mathrm{e} = (1 - \beta^2)^2 \tag{4}$$

In equation (3), the velocity in the duct immediately before the abrupt enlargement is used.

When fluid flows through an abrupt contraction a vena contracta is formed in the pipe directly downstream of the contraction. A region of separated flow is formed between the vena contracta and the wall, and most of the loss of total pressure takes place in the downstream expansion of the flow cross-sectional area from the vena contracta to that of the duct [25]. The pressure loss can be calculated from equation (5)

$$\Delta p_c = \frac{1}{2} k_c \rho u_o^2 \tag{5}$$

$$k_c = -0.33\beta^{-2} - 0.18\beta^{-1} + 0.5 \tag{6}$$

In equation (5), the velocity in the duct immediately after the abrupt contraction is used. In equation (6), we have fitted a quadratic polynomial to the empirical data for k_c given in reference [25].

2.2.3 Changes in the flow direction

When fluid flows along a curved path a radial pressure gradient forms to provide the necessary centripetal acceleration. This results in an increase in pressure towards the outside of the bend and a decrease in pressure along the inside of the bend. A pressure maximum occurs at the midpoint of the bend on the outer side and a pressure minimum occurs on the inner side of the bend adjacent to this. This state necessitates the existence of two adverse pressure gradients – one on the outer side of the bend before the midpoint and one on the inside of the bend after the midpoint. If the curvature of the bend is sufficiently severe these adverse pressure gradients can cause flow separation with the associated total pressure losses.

The pressure gradients in the bends also cause secondary flows in the form of counter-rotating eddies whose effect is superimposed onto the primary flow field. The effect of these eddies can persist downstream for up to 75 times the pipe diameter [25]. Crawford *et al.* [26] present a method to estimate the total pressure losses caused by a bend if the bend radius, pipe diameter, Reynolds number, and surface friction factor are known.

2.2.4 Faulty seals leading to leakage of fluid to the atmosphere

The static pressure inside the inlet duct is higher than atmospheric pressure. This means that if the duct is not properly sealed fluid will leak to the atmosphere. Any fluid which escapes to the atmosphere bypasses the nozzle and performs no useful work. Two major potential leak paths exist in the turbine. First, fluid could leak at the interface of the nozzle insert and the turbine housing (as shown in Fig. 1(c)); second, a part of the jet may not enter between the discs, thus bypassing the rotor.

Table 1 Calculated loss coefficients for inlet and nozzle

Loss mechanism	Loss coefficient
Friction against wall	0.27
Changes in inlet duct diameter in three places (all referred to the velocity in the 6 mm diameter section)	0.86
90° bend in the elbow	1.65
90° bend in the nozzle	0.94

2.3 Relative magnitude of different loss mechanisms in the inlet

Using the empirical methods presented in section 2.2 the pressure loss coefficients for the inlet duct and nozzle are estimated. Table 1 shows the calculated loss coefficients of the various sections and flow features in the inlet and nozzle. The above formulae are valid only for incompressible flow. For a nozzle exit area of 1.5×6.3 mm, a simple one-dimensional (1D) isentropic analysis estimates the Mach number in the inlet duct to be within the incompressibility limit. However, as the nozzle exit area is increased, the Mach number in the duct increases and the flow would need to be treated as compressible. There are also unknown quantities of leakage, which increases with increasing pressure in the system. (Direct measurement of the mass flowrate at the inlet and the exit of the turbine can determine the overall leakage, but such instrumentation was not available for the present investigation.) Thus, it is difficult to estimate the exact loss empirically. The empirical analysis, however, brings out the relative magnitudes of losses and the qualitative physics well. It also shows that a significant amount of loss can be incurred in a relatively short inlet that is designed not keeping the loss mechanisms in perspective. At any rate, the actual overall loss has been measured experimentally in this work.

2.4 Performance of the nozzle

2.4.1 Background

The purpose of a nozzle is to convert energy stored in the form of pressure into directed kinetic energy. For subsonic flow, this is achieved by reducing the duct area in the direction of the flow [27]. This induces a favourable pressure gradient causing the fluid to be accelerated through the nozzle. Separation is not expected because of the presence of the favourable pressure gradient; as a result, the efficiency of nozzles is usually very high often exceeding 96 per cent [28, 29].

For small-sized nozzles with throat widths of less than 3 mm, the boundary layer can occupy a significant portion of the nozzle area [30]. Flows in these nozzles are characterized by small Reynolds numbers ($Re < 10^5$) and are laminar [30]. The relative thickness

of the boundary layer can result in reduced nozzle performance because of increased viscous losses [31]. In nozzles of this kind it is found that total pressure losses decrease as the Reynolds number of the flow increases [30], since the thickness of the boundary layer decreases with increasing Reynolds number.

2.4.2 Ratio of total pressures

The total pressure remains constant in isentropic flow in the absence of work transfer. For a real adiabatic flow without work transfer losses due to friction manifest themselves as a drop in total pressure. Benedict *et al.* [32] states that the ratio of total pressures is a significant but little discussed parameter which gives a clear thermodynamic indication of the loss in terms of entropy. When studying nozzle performance the use of this parameter is convenient when an accurate measurement of stagnation temperature is not possible.

$$\Re_{\text{nozzle}} = \frac{\bar{p}_{0\text{o}}}{\bar{p}_{0\text{i}}} \tag{7}$$

$\Re_{\text{nozzle}}$ is calculated here by dividing the outlet gauge total pressure by the inlet gauge total pressure. Gauge total pressure is used because it represents the energy available to do useful work (i.e. although fluid with an absolute pressure of 1 bar has energy in the form of pressure, this energy cannot be usefully extracted).

2.4.3 Effects of 90° bend combined with a change in flow cross-sectional area

The loss in total pressure is not the only relevant parameter in assessing the performance of the nozzle, but we argue that there are also other important features such as the flow uniformity over the nozzle outlet area that characterize the overall performance of the nozzle.

As stated in section 2.1.2, the exit plane of the nozzle is at 90° to the plane of the inlet. It is known that a 90° bend in a duct will distort the velocity profile in the jet causing higher velocity flow around the outside of the bend and low velocity flow on the inside [28]. This is not desirable for the nozzle in a disc turbine because it would cause some discs to see a higher mass flowrate than others. However, although there is literature describing the flow characteristics of a pipe of constant cross-section undergoing a 90° bend, it is not known how the presence of a contraction (the nozzle in the present case) and resulting favourable pressure gradient directly after the 90° bend would affect the flow field.

2.4.4 Computational investigation of nozzle exit flow uniformity

It was therefore decided to carry out a CFD simulation of the flow field in the nozzle. Analysis was carried out using a Navier–Stokes code with turbulence modelling ($k-\varepsilon$) in FLUENT [33]. Geometry and Cartesian meshes were generated using Gambit [34].

The cross section of the inlet portion of the nozzle is circular but the nozzle exit cross section is rectangular. This meant that it was not possible to create a 2D model by taking a 2D slice of the nozzle. It was necessary to create a 2D model of the nozzle insert that maintained the most important characteristics of the real flow. The two most important parameters which needed to be modelled were the geometry (i.e. the 90° bend, and the reduction in cross-sectional area caused by the nozzle). The ratio of nozzle inlet to exit area was represented in the 2D model as the ratio of nozzle inlet to exit width. As far as possible the rest of the 2D geometry was based on the dimensions of the real nozzle insert.

Three cases were studied to replicate the conditions found in different Tesla turbine nozzles and these are summarized in Table 2:

Case (a): 1.5 × 6.3 mm plenum-integrated nozzle. The fluid from a stationary state inside an infinite reservoir exits through the nozzle. It would be expected that the flow in the jet would be very uniform with little loss in total pressure. This case was used as a benchmark to compare the other cases against.

Case (b): 1.5 × 6.3 mm original nozzle. This case represents a nozzle that has an inlet to exit area ratio of 3.0. A nozzle of this type was used in most tests reported by Hoya and Guha [3] as it allowed a rotor containing six discs to be tested. This case should demonstrate the effect of the pressure gradients caused by a 90° bend coinciding with the favourable pressure gradient caused by an area contraction.

Case (c): 2.0 × 20 mm original nozzle. This case shows the effect of using a nozzle where the exit area is larger than the inlet area – this kind of nozzle was used when testing the rotor with a large number of discs. In this case, the favourable pressure gradient associated with the nozzle is removed.

Details of the CFD investigation and results for the above cases are given in Appendix 2.

Table 2 Summary of CFD tests runs on flow field in the nozzle

Case	Flow type	Width (mm)	Length (mm)	Inlet area (mm^2)	Exit area (mm^2)
(a)	Reservoir	1.5	6.3	Infinite	9.45
(b)	Duct flow with 90° bend	1.5	6.3	28.3	9.45
(c)	Duct flow with 90° bend	2.0	20	28.3	40.0

2.5 Notes on inlet performance

2.5.1 Choking upstream of the nozzle

Choking occurs when the ratio of inlet total pressure to outlet static pressure across a converging flow passage becomes higher than a certain value, the limiting ratio is 1.89 for the isentropic flow of a perfect gas of isentropic index 1.4 (air) [25]. At choked conditions, the flow velocity at the minimum cross-section becomes sonic and the non-dimensional mass flowrate cannot rise any further (if no variation in p_0 or T_0 occurs).

In the test rig, it was found that for some of the nozzles, the inlet area (which was fixed for all cases to have a common connection to the compressed air supply) was smaller than the nozzle outlet area (which was varied according to how many discs were used in the test Tesla turbine). This meant that choking would occur in the duct upstream of the nozzle rather than at the throat of the nozzle. This is undesirable for several reasons.

1. The flow velocity in the duct would be high. Since pressure losses increase with the square of the velocity, as shown by equation (1), this would lead to high total pressure losses [24].
2. The losses in total pressure in small nozzles decrease as the Reynolds number increases [30]. Thus, the best performance would be reached when the flow velocity through the nozzle reached its maximum value. If the flow chokes upstream of the nozzle the maximum velocity through the nozzle may not be reached.
3. The supposed 'nozzle' would act as a diffuser.

Choking upstream of the nozzle may also mean that a convergent–divergent passage may be formed, and hence supersonic flow may occur. This needs further investigation.

2.5.2 Difficulty of determining stagnation pressure at nozzle inlet

Another problem faced by previous investigators using this turbine [3] was that, due to geometric constraints, it was not possible to measure the total pressure exactly at the inlet of the nozzle. The closest place where the measurement could be made was in the elbow fitting upstream of the nozzle. There were a few abrupt changes in the flow cross-sectional area between the elbow fitting and the nozzle. Hoya and Guha [3] used empirical methods to estimate the pressure drop, but accuracy of this method for a compressible flow regime is not clear.

3 DESIGN OF NEW INLET

It has been shown that the Tesla turbine's inlet and nozzle can be responsible for significant losses. Here

a design methodology has been formulated to reduce these losses by integrating a plenum chamber with the inlet of the Tesla turbine.

3.1 Requirements of plenum chamber inlet for a Tesla turbine

From studies reported in references [3] and [10], and the available literature, a number of design requirements have been identified to which an improved nozzle design must conform.

1. The nozzle must provide similar mass flow to each disc passage.
2. The nozzle and inlet demonstrate low total pressure losses over the inlet pressure range used by the turbine.
3. Multiple different nozzle geometries must be able to be tested without modifying the inlet or turbine.
4. It must be possible to test the efficiency of the nozzle separately to the efficiency of the whole turbine.
5. The inlet must allow the total pressure and temperature to be measured directly before the nozzle.

3.2 Working principles and design of plenum chamber

A plenum chamber is a high pressure settling tank in which a fluid is brought to near-stagnation state. By the principle of conservation of mass this necessitates a large increase in flow cross-sectional area.

Although plenum chambers are common components in many engineering systems [35] there is little discussion in the literature devoted to them. This fact is commented upon by Lau *et al*. [36]. There is no guidance on how a plenum chamber should be designed or how the design of a plenum chamber would affect its performance. Several investigations, however, have been made into the pressure loss caused by cylindrical plenum chambers with aligned and non-aligned inlets and exits [36, 37].

3.2.1 Character of flow in a plenum chamber

Harrison and Klemz [38] conducted a computational study into the flow in plenum chambers by numerically solving the 2D Navier–Stokes equations with turbulence modelling using a finite difference scheme. They concluded that the flow inside the plenum chamber could be termed as re-circulating since the flow had no dominant direction. Sparrow and Bosmans [37] found experimentally that the pressure loss in the plenum chamber was insensitive to Reynolds number from which they concluded that inertial losses dominate frictional losses. They also found a large swirling component in the fluid in the plenum chamber. When studying the pressure loss caused by a cylindrical plenum chamber with axially aligned inlet

and outlet, Lau *et al.* [**36**] found that, in the range tested $l/d < 10$, the pressure loss was always lower than the loss expected for the combined effects of an abrupt enlargement and an abrupt contraction occurring separately. They also found that the pressure loss in the plenum chamber increased with the length of the plenum chamber. This suggests that, as the plenum's length increases, the abrupt enlargement and contraction assert their separate identities to a greater extent (i.e. the flow loses the character given to it by the abrupt enlargement and becomes more uniform (like a fully developed pipe flow)).

Although the above details provide a description of the flow structure inside a plenum chamber, they do not provide the analytical tools necessary to design a plenum chamber.

3.2.2 Description of new plenum-integrated nozzle

In order to address the paucity of information in the literature, a new approach for the design of the plenum chamber was formulated, which is described in Appendix 3. A finite difference approach to solve the 1D isentropic flow equations was used to predict the time-variation and steady state values of all flow variables at different key points in the flow field, including the velocity of the flow at the inlet to the plenum chamber. The results from this analysis showed that for a nozzle with a $h = 6.3$ mm and $w \leqslant 3$ mm, the velocity of the flow in the plenum inlet was sufficiently small that the fluid could be considered incompressible. The diameter ratio required to produce a near stagnant flow inside the plenum chamber was calculated with two different approaches – continuity equation and pipe flow loss equations. This analysis showed for a diameter ratio of 0.04 the difference between the total and stagnation pressure would be of the order of 0.1 per cent. The length required for reattachment was predicted using experimental sudden enlargement data [**39**]. Full details of this approach can be found in Appendix 3. The final dimensions of the designed plenum chamber are as follows: inlet diameter 6 mm, plenum diameter 25 mm, plenum length 150 mm. Stress calculations were undertaken to ensure that the plenum chamber would be able to contain pressures of up to 10 bar safely.

The plenum chamber was manufactured and tested with the old and new nozzles. The results are presented in section 4.

3.2.3 Integration of plenum chamber into existing turbine rig

The experimental results presented in this paper concentrate on the performance of various nozzle–inlet assemblies. The purpose of the present design and testing was to prove the concept of using a plenum chamber as the inlet of a Tesla turbine.
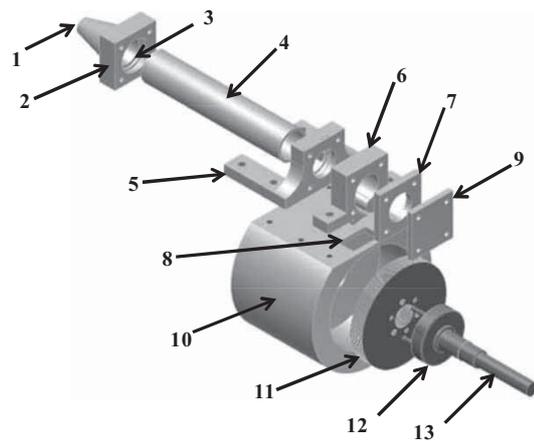
Fig. 2 Expanded view of the conceptual design for the plenum chamber integration with turbine casing. Keys: (1) inlet, (2) diffuser, (3) groove for O-ring, (4) plenum chamber, (5) attachment to turbine housing, (6) integrated nozzle, (7) spacer, (8) slot in turbine casing, (9) end plate sealing plenum chamber, (10) turbine housing, (11) disc rotor, (12) spindle, and (13) axle

Figure 2 shows the expanded view of a conceptual design assembly for integrating the plenum chamber with the turbine casing. The turbine base-plate which holds the rotor has been excluded from the diagram to allow the rotor and spindle to be fully visible. It would be necessary to modify the turbine casing for the new plenum chamber to be attached. One edge of the casing is planed flat and a hole is cut into the casing to expose the discs (this could be achieved by a CNC machine). The nozzle has a keyed section which slots into the hole in the turbine casing allowing the fluid to be injected onto the turbine. Flanges extending from the plenum chamber allow the chamber to be bolted to the turbine. The whole assembly would be sealed by a custom-made gasket. Because the turbine is primarily impulsive, the internal static pressure is not significantly elevated above atmospheric pressure. This means that sealing between the plenum chamber and the casing is important but not as critical as ensuring that the inlet of the plenum chamber is sealed.

3.2.4 Estimating losses at the inlet of plenum chamber integrated in a Tesla turbine

For the purpose of the present study which centres on the design and performance of the nozzle, the inlet to the plenum chamber was left as an abrupt enlargement. However, when building a real Tesla turbine incorporating the plenum chamber, a diffuser should be used at the inlet of the plenum chamber, as shown in Fig. 2. This would allow the majority of the kinetic energy of the flow to be conserved and converted into static pressure. Zaryankin [**40**] provides a method to determine the losses associated with a diffuser by way

of formulating a friction factor that takes into account the two main sources of loss in diffusers: friction losses and expansion losses. Using this method, the maximum pressure loss which would be experienced in a normal plenum operation is of the order of 0.03 bar.

3.3 Summary of the features on the designed plenum chamber

A plenum chamber inlet with integrated nozzle has been designed in such a way that the problems identified with the original turbine inlet nozzle in section 2.2 are mitigated. The plenum provides a near stagnant flow directly before the nozzle which eliminates the large pressure gradient identified in the original nozzles. This improves the uniformity of the flow across the nozzle outlet area and reduces losses in total pressure. This design also allows accurate measurement of the stagnation pressure and temperature directly before the nozzle allowing the percentage stagnation pressure loss over the nozzle to be accurately determined. The plenum chamber design allows the efficiency of the nozzle to be measured individually which would allow the efficiency of the disc rotor to be directly inferred.

4 RESULTS AND DISCUSSION

Two principal experimental set-ups and results are presented here on the performance of nozzles and inlets. The first line of investigation centred around the loss of total pressure in various nozzle–inlet assemblies. The test rig for this aspect of the study is shown in Fig. 1. The second line of investigation centred around the uniformity of the jet over the cross section of the nozzle outlet. The experimental set-up for this part of study is shown in Fig. 3.

4.1 Efficacy of various nozzle–inlet assemblies

The losses associated with different nozzles and inlets were tested in three scenarios to try to gain the best insight into where the losses were occurring.

1. *Original nozzle and turbine inlet assembly*: in this test, the efficiency of the nozzle was tested inside the turbine casing, replicating the conditions seen by the nozzle in normal turbine operation. This test demonstrated the extent to which poor nozzle performance would impact on the measured efficiency of the whole machine.
2. *Original nozzle with plenum inlet*: the original nozzles were bolted to the new plenum chamber inlet. This allowed the performance of the old nozzles on their own to be measured as the inlet now provided negligible losses.
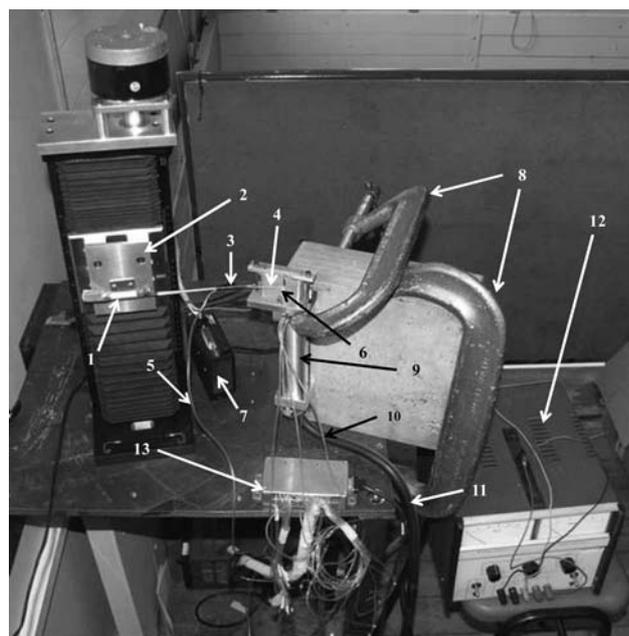
Fig. 3 Experimental set-up for performing total pressure traverses. Keys: (1) clamp on traverse, (2) travelling element, (3) bar supporting Pitot probe, (4) Pitot probe, (5) tube transmitting nozzle exit total pressure, (6) nozzle, (7) controller interfacing the traverse with the computer, (8) G clamps stabilizing assembly, (9) plenum chamber, (10) tube transmitting plenum total pressure, (11) supply line from cylinder, (12) traverse power supply, and (13) Scanivalve

3. *New plenum-integrated nozzle*: the new plenum-integrated nozzle was tested to determine the extent of the efficiency improvement that could be achieved by using a plenum chamber.

Air was used as the working fluid and was provided by a high pressure cylinder with a maximum pressure of 200 bar. This was reduced to the range 0–10 bar by a two-stage pressure regulator. Air was delivered to the turbine via 8 mm pneumatic tubing. For the turbine inlet, stagnation and static pressure measurements were taken at an elbow fitting directly before the fluid entered the turbine casing. For the plenum chamber, pressure measurements were taken by two pressure tappings – one pointing axially and the other radially. The outlets from the pressure tappings were delivered to a ZOC 22B Scanivalve via thin flexible tubing. The ZOC 22B Scanivalve has a full scale accuracy of 0.1 per cent over the range 0–3.6 bar gauge pressure [41].

4.1.1 Comparison of inlet performances for 1.5 mm nozzle

Figure 4 shows a comparison of the 1.5 mm nozzle for the three different testing procedures outlined in section 4.1. It can be seen that, for the original nozzle,
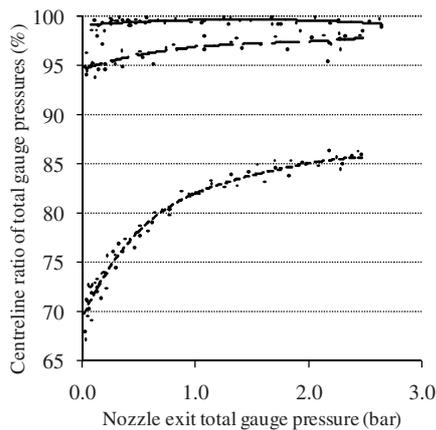
Fig. 4 Comparison of performance of 1.5 × 6.3 mm nozzle with different inlets. Keys: ——— (top) new plenum-integrated nozzle, ——— (middle) original nozzle with plenum inlet, and — — — — — — (bottom) original nozzle with turbine inlet assembly

the total pressure ratio across the nozzle increases with increasing inlet pressure. This is because as the inlet pressure increases, the Mach number of the flow in the nozzle increases. This causes the boundary layers to become thinner which reduces the viscous losses in the nozzle [30, 31]. After the flow is choked, the static pressure of the jet at the nozzle exit increases with increasing nozzle inlet total pressure, which results in an increased fluid density in the nozzle. Consequently the Reynolds number of the flow increases monotonically with increasing supply pressure when the nozzle outlet area is kept fixed. This manifests itself in the loss in total pressure decreasing monotonically with supply pressure. For the new plenum-integrated nozzle, the loss in total pressure is very low and there is scatter in the data, making it difficult to rationalize any trend.

Comparing the performance of the different inlets, it can be seen that the original nozzle and turbine assembly has the poorest performance and the plenum-integrated nozzle has the highest performance. Table 3 summarizes the loss in total pressure, as percent of nozzle inlet total pressure, for various inlet-nozzle

Table 3 Comparison of loss in total pressure, as percent of nozzle inlet total pressure, for various inlet–nozzle assemblies (1.5 × 6.3 mm nozzle exit)

Total pressure at nozzle inlet (bar)	% loss in total pressure		
	Original nozzle and turbine assembly	Original nozzle with plenum inlet	New plenum-integrated nozzle
1.5	23	4	0.5
3.5	14.5	2.3	0.4

assemblies (1.5 × 6.3 mm nozzle exit). Results are tabulated at two inlet total pressure values, 1.5 and 3.5 bar. As compared to the original nozzle and turbine assembly, the new plenum-integrated nozzle has reduced the loss by a factor of about 40–50 (an improvement of 4000–5000 per cent).

By comparing the values in the second and the third columns of Table 3, it can be seen that it is the original inlet that is responsible for the majority of losses. This shows that the original nozzle even with the 90° bend has a reasonable efficiency. This is consistent with the prediction made in section 2.4 that the favourable pressure gradient caused by the nozzle would, to some extent, offset the adverse pressure gradients created by the 90° bend. By comparing the values in the last two columns of Table 3, it is seen that significant further reduction in total pressure loss is achieved by the removal of the 90° bend within the nozzle.

4.1.2 Comparison of inlet performances with varying nozzle width

Similar experiments as in section 4.1.1 were conducted for nozzles of different widths. The new plenum-integrated nozzle maintained a total pressure loss below 1 per cent for all nozzles tested – up to 3 mm width. For the original nozzle with turbine inlet assembly, the loss in total pressure increased further by a significant amount as nozzle width increased. This is because as the nozzle area gets closer to the duct area the flow velocity in the duct gets closer to the jet velocity. This significantly increases losses due to changes in the pipe direction and changes in the pipe cross-sectional area because these losses scale with the square of the velocity. Thus, the difference in total pressure loss between the original inlet and the new plenum-integrated nozzle would be much higher than what is shown between the second and fourth columns of Table 3 when the nozzle outlet area increases.

4.1.3 Summary of results on efficacy of nozzle–inlet assemblies

The inlet and nozzle were responsible for significant pressure losses in the turbine. Most of this loss was due to abrupt changes in area and the 90° elbow in the inlet, and the 90° bend in the nozzle. This conclusively shows that the inlet and nozzle to the Tesla disc turbine need not be 'long and inefficient' as was concluded in reference [2].

4.2 Pitot tube traverse results to assess the uniformity of jets

So far the performance comparison between the nozzles has been made by comparing the ratio of centreline total pressures. In reality, the comparison should be made between the average total pressure across the

flow before and after the nozzle as this accounts for the fact that the total pressure is not constant across the jet or the inlet. In order to assess the extent of flow non-uniformity and to ascertain the extent to which a single Pitot tube measurement at an approximately centre-line position represents averaged value, Pitot tube traverses were conducted in both directions (width and height) over the nozzle outlet area. The experimental set-up is shown in Fig. 3. This involved using a high precision traverse mechanism, which is digitally precision-controlled through a computer.

The non-uniformity in total pressure is caused by two major effects. Bends in the inlet and within the nozzle distorts the flow as explained in section 2. This will be more prevalent in the height-wise direction in the original nozzle and turbine assembly. The action of viscosity (wall effect) also creates non-uniformity in total pressure. As a percent of nozzle dimension this will be more pronounced in the direction of nozzle width (since the widths of the nozzles are smaller than their respective heights).

Figure 5 and Table 4 show illustrative results for three nozzle–inlet assemblies. Table 4 shows how effectively a Pitot tube approximately positioned at the centre would record a value close to the true centre-line total pressure. From Fig. 5 it can be seen that the nozzle and inlet has a very definite impact on the uniformity of the flow from the nozzle. As would be expected, the plenum chamber has a very symmetrical profile. The original nozzles that incorporate the 90° bend tend to have a higher total pressure towards the outside of the bend. This is far more apparent on the nozzle with a 20 mm width. This is because the outlet area of that nozzle is larger than the nozzle entrance, this means that there is no contraction and therefore
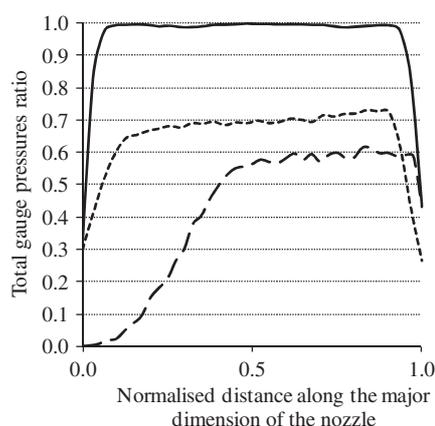
Table 4 Comparison of area over which Pitot measurement is approximately representative of actual centre-line total pressure as a function allowable maximum error

Maximum error (%)	Central portion of jet as % of height over which the variation in total pressure is within the error limit		
	Plenum-integrated nozzle 1.5 × 6.3 mm	Original nozzle with turbine assembly 1.5 × 6.3 mm	Original nozzle with turbine assembly 2 × 20 mm
1	81	32	10
2	87	45	20
3	87	54	35
4	87	61	52
5	87	74	52

no favourable pressure gradient. In contrast to this, the 1.5 mm nozzle has a much less distorted profile because the favourable pressure gradient caused by the nozzle counteracts the adverse pressure gradients caused by the sudden bend. These results match and verify the 2D CFD results discussed in Appendix 2.

The greater the flow non-uniformity, the greater would be the difference between the centre-line total pressure and the area-weighted value. Since in quasi-1D analysis of performance of turbines and nozzles only one representative value is used at each section of the flow path, efficiencies calculated on the basis of the centre-line values may be significantly different from their true values (if the flow non-uniformity is severe). The effects of non-uniformity on area-weighted total pressures, for various nozzle–inlet assemblies, are discussed in Appendix 2. The results in Appendix 2 show that for a badly designed nozzle the actual performance would be much worse than the efficiency calculated using centre-line total pressure values.

5   CONCLUSION

In this work, the performance of the inlet to a Tesla disc turbine has been thoroughly studied and the causes of loss have been established. It has been shown that the nozzle and inlet are responsible for a large proportion of the losses in traditional designs of a Tesla turbine. The work reports on how to significantly improve the performance of the inlet and the nozzle, in the past the poor performance of which has often been assumed to be unavoidable [2].

A new nozzle utilizing a plenum chamber inlet has been designed and tested. Experiments have demonstrated less than 1 per cent loss in total pressure in the new design compared to losses in the range 13–34 per cent for the original nozzle and inlet. As compared to the old inlet–nozzle assembly, the new design reduced the loss in total pressure by a very large factor (40–50). This would significantly improve the overall efficiency of the Tesla disc turbine. This result

Fig. 5 Results from experimental total pressure traverses along the major dimension of the nozzle outlet. Keys: ——— 1.5 × 6.3 mm plenum-integrated nozzle, - - - - - 1.5 × 6.3 mm original nozzle, and —— 2.0 × 20.0 mm original nozzle (for these tests, the inlet centre-line total gauge pressure is 0.5 bar)

shows that the suggestion in the literature that the nozzle and inlet were responsible for significant losses is true but that the nozzle and inlet can, with careful design, perform very efficiently.

Other than the dramatic improvement in loss reduction, the new plenum-integrated nozzle achieves a considerable enhancement in the uniformity of the jet. This has been demonstrated here both by experimental traverses of Pitot tubes as well as CFD studies. The greater uniformity of the jet means that a single Pitot measurement approximately positioned at the centre of the jet would record a value close to the true centre-line total pressure, and that calculations based on centre-line values of total pressure would give, to a good accuracy, the area-averaged loss coefficient of the nozzle–inlet assembly. The uniformity of the jet also means that all disc passages would receive uniform inlet conditions; this should improve the performance of the rotor thereby further enhancing the overall efficiency of the Tesla turbine.

A design has been put forward which would allow the plenum chamber and nozzle to be integrated with the current turbine with only minimal changes to the casing being required. By interchanging the nozzle with other different geometries, it would be easy to study how the way in which the fluid is injected into the rotor affects the overall machine efficiency.

This design paves the way for the efficiency of the rotor to be determined experimentally for the first time. Up till now, experimenters have measured the overall efficiency of the whole turbine. Since this figure included nozzle losses, rotor losses, and exhaust losses, it was difficult to determine quantitatively which component was responsible for the poor performance of the turbine. With a nozzle that can be removed from the turbine casing, the nozzle efficiency can be determined in isolation thus allowing the rotor efficiency to be inferred more accurately.

ACKNOWLEDGEMENTS

REFERENCES

1 **Rice, W.** An analytical and experimental investigation of multiple-disk turbines. *J. Eng. Power*, 1965, **87**(1), 29–36.

2 **Rice, W.** Tesla turbomachinery. In *Handbook of turbomachinery* (Ed. E. Logan), 2003, pp. 861–874 (Marcel Dekker, New York).

3 **Hoya, G. P.** and **Guha, A.** The design of a test rig and study of the performance and efficiency of a Tesla disc turbine. *Proc. IMechE, Part A: J. Power and Energy*, 2009, **223**(A4), 451–465. DOI: 10.1243/09576509JPE664.

4 **Tesla, N.** *Fluid propulsion*. US Patent 1,061,142, May 1913.

5 **Tesla, N.** *Turbine*. US Patent 1,061,206, May 1913.

6 **Cairns, W. M. J.** *The Tesla disc turbine*, 2003 (Camden Miniature Steam Services, Great Britain).

7 **Armstrong, J. H.** *An investigation of the performance of a modified Tesla turbine*. MS Thesis, Georgia Institute of Technology, June 1952.

8 **Beans, E. W.** Investigation into the performance characteristics of a friction turbine. *J. Spacecr.*, 1966, **3**(1), 131–134.

9 **Davydov, A. B.** and **Sherstyuk, A. N.** Experimental research on a disc microturbine. *Russ. Eng. J.*, 1980, **60**(8), 19–22.

10 **McGarey, S.** and **Monson, P.** Performance and efficiency of disk turbines. MEng research project report no. 1203, University of Bristol, 2007.

11 **Guha, A.** Optimisation and design of aero gas turbine engines. *Aeronaut. J.*, 2001, **105**(1049), 345–358.

12 **Guha, A.** A unified theory of aerodynamic and condensation shock waves in vapour-droplet flows with or without a carrier gas. *Phys. Fluids*, 1994, **6**(5), 1893–1913.

13 **Guha, A.** Structure of partly dispersed normal shock waves in vapour-droplet flows. *Phys. Fluids A*, 1992, **4**(7), 1566–1578.

14 **Guha, A.** Jump conditions across normal shock waves in pure vapour-droplet flows. *J. Fluid Mech.*, 1992, **241**, 349–369.

15 **Guha, A.** A unified theory for the interpretation of total pressure and temperature in two-phase flows at subsonic and supersonic speeds. *Proc. R. Soc.*, 1998, **454**, 671–695.

16 **Guha, A.** Computation, analysis and theory of two-phase flows. *Aeronaut. J.*, 1998, **102**(1012), 71–82.

17 **Lawn Jr, M. J.** and **Rice, W.** Calculated design data for the multiple-disk turbine using incompressible fluid. *Trans. ASME, J. Fluids Eng.*, 1974, **96**, 252–258.

18 **Allen, J.** Examining the Tesla turbine. In Proceedings of the 27th Aerospace Sciences Meeting, Reno, NV, 9–12 January 1989, AIAA Paper 89–0838.

19 **Mattingly, J. D.** *Elements of gas turbine propulsion*, 1996 (McGraw Hill International Editions, Singapore).

20 **Cohen, H., Rogers, G. F. C.,** and **Saravanamuttoo, H. I. H.** *Gas turbine theory*, 4th edition, 1996 (Longman Group Ltd, Cornwall).

21 **Guha, A.** Performance and optimization of gas turbines with real gas effects. *Proc. IMechE, Part A: J. Power and Energy*, 2001, **215**(A4), 507–512. DOI: 10.1243/0957650011538631.

22 **Guha, A.** An efficient generic method for calculating the properties of combustion products. *Proc. IMechE, Part A: J. Power and Energy*, 2001, **215**(A3), 375–387. DOI: 10.1243/0957650011538596.

23 **Guha, A.** Optimum fan pressure ratio for bypass engines with separate or mixed exhaust streams. *AIAA J.*, 2001, **17**(5), 1117–1122.

24 Crane. *Flow of fluids through valves, fittings and pipes,* 1982 (Crane Co., New York).

25 Massey, B. *Mechanics of fluids,* 8th edition, 2006 (Taylor & Francis, Oxon).

26 Crawford, N. M., Cunningham, G., and **Spedding, P. L.** Prediction of pressure drop for turbulent fluid flow in 90° bends. *J. Process Mech. Eng.*, 2003, **217**, 153–155.

27 Anderson Jr, J. D. *Fundamentals of aerodynamics,* 3rd edition, 2001 (McGraw Hill, New York).

28 Shepherd, D. G. *Principles of turbomachinery,* 1956 (The Macmillan Company, New York).

29 Shames, I. H. *Mechanics of fluids,* 4th edition, 2002 (McGraw-Hill Professional, New York).

30 Butenko, V. A., Rylov, Y. P., and **Chikov, V. P.** Experimental investigation of the characteristics of small-sized nozzles. *Izv. Akad. Naur SSSR*, 1976, **6**, 137–140.

31 Whalen, V. M. *Low Reynolds number nozzle flow study.* MS Thesis, NASA technical memoranum, 1987.

32 Benedict, R. P., Carlucci, N. A., and **Swetz, S. D.** Flow losses in abrupt enlargements and contractions. *J. Eng. Power*, 1966, **88**, 73–81.

33 Fluent Inc. *FLUENT 6.3 user's guide,* 2003–2004 (Fluent Inc., Lebanon).

34 Fluent Inc. *Gambit user's guide,* 2009, available from http://web.njit.edu/topics/Prog_Lang_Docs/html/FLUENT/fluent/gambit/help/users_guide/ugtoc.htm.

35 Williams, G. H. *Homebuilt hovercraft,* Flight International Supplement, 28 January 1965.

36 Lau, S. C., Sparrow, E. M., and **Ramsey, J. W.** Effect of plenum length and diameter on turbulent heat transfer in a downstream tube and on plenum-related pressure losses. *J. Heat Transfer*, 1981, **103**, 415–421.

37 Sparrow, E. M. and **Bosmans, L. D.** Heat transfer and fluid flow experiments with a tube fed by a plenum having nonaligned inlet and exit. *Trans. ASME, J. Heat Transfer*, 1983, **105**, 56–62.

38 Harrison, J. A. and **Klemz, B. L.** An investigation of the steady fluid flow within a simple plenum chamber. *High-Speed Surf. Craft*, 1982, 32–34.

39 So, R. M. C. Inlet centerline turbulence effects on reattachment length. *Exp. Fluids*, 1987, **5**, 424–426.

40 Zaryankin, A. E. A note on calculating losses in diffuser elements. *Inz.-Fiz. Zh.*, 1965, **8**(4), 531–535.

41 Scanivalve Corp. ZOC 22B electronic pressure scanning module, instruction and service manual, 2005, available from Scanivalve site www.scanivalve.com.

APPENDIX 1

Notation

a speed of sound
A cross-sectional area
d diameter
F friction factor
h Nozzle's major dimension (height)
H enlargement step size $= (d_o - d_i)/2$
k pressure loss coefficient
l length
$\dot{m}$ mass flowrate
M mach number

n time step
p absolute static pressure
p_0 absolute total pressure
$\bar{p}$ gauge pressure
Δp change in total pressure
R gas constant
t time
T static temperature
u velocity
w Nozzle's minor dimension (width)
x_L reattachment length

β diameter ratio $= d_i/d_o$
Δ change in quantity
Φ static to total pressure ratio $= p/p_0$
ρ fluid density
γ ratio of specific heats
$\Re$ ratio of total gauge pressures $= \bar{p}_{0o}/\bar{p}_{0i}$

Subscripts

c   duct contraction loss
e   duct expansion loss
f   friction loss
i   inlet
o   outlet

APPENDIX 2 CFD STUDY OF THE FLOW IN THE INLET AND NOZZLE

As was described in section 2.4.4, CFD analysis with FLUENT was undertaken to provide insight into the flowfield in three different nozzle–inlet combinations. Simulations were run with a nozzle inlet total pressure of 1.56 bar, the jet discharging into atmosphere. The total temperature was taken to be 288 K. The solution was considered to have converged when the residuals were below 1e-6.

Figure 6 shows the predictions of FLUENT for the three geometries. The contours of total gauge pressure are shown. The plenum-like nozzle produces a very uniform jet with low losses in total pressure. Both nozzles that incorporated the 90° bend at the outlet had flow separation at the inside edge and a higher total pressure on the outside than the inside. This fits with the experimental results (section 4.2) and the theory that was presented in section 2.2. The total pressure profile of the nozzle with a height of 20 mm was more severely distorted than the nozzle with a 6.3 mm height. It has been explained in section 2.2.3 that the outlet area of the nozzle with a height of 20 mm is greater than the area of the inlet duct and hence the counterbalancing effect of a favourable pressure gradient that is usually present in a nozzle is not present here.

Figure 7 shows the variation of total pressure ratio across the major dimension of the three nozzles as
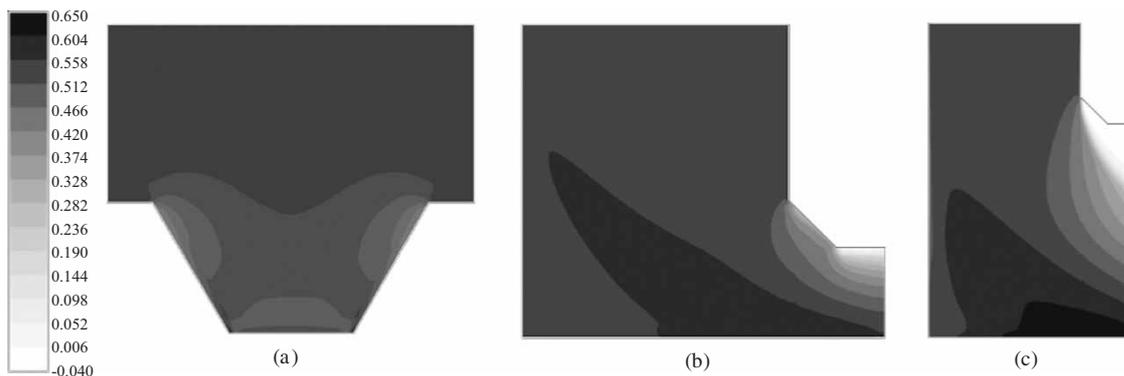
Fig. 6 Total gauge pressure contour plots for various nozzles, results of CFD analysis. Keys: (a) 1.5×6.3 mm plenum-integrated nozzle (flow from top to bottom), (b) 1.5×6.3 mm original nozzle (flow from top to lower right), and (c) 2.0×20 mm original nozzle (flow from top to right)
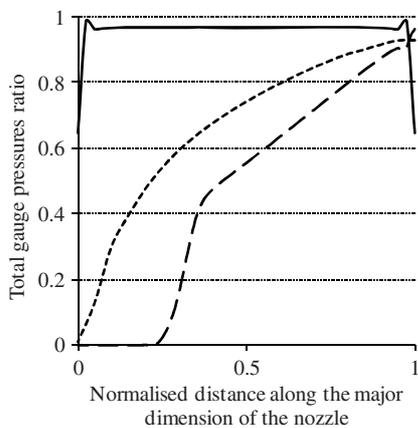
Fig. 7 Total pressure profiles at nozzle exit, results of CFD analysis. Keys: ——— 1.5×6.3 mm plenum-integrated nozzle, - - - - 1.5×6.3 mm original nozzle, and ——— 2.0×20 mm original nozzle

predicted by the CFD simulations. This can be compared with Fig. 5, where the measured values of the same quantities were plotted. There is good qualitative agreement between the experimental and computational results. Area-weighted average total pressure was calculated from the CFD results for the three geometries and is presented in Table 5.

Table 5 shows that there is very close agreement between the CFD and experimental results for the two nozzles with a height of 6.3 mm. This shows that the 2D CFD model in these cases sufficiently captures the most salient characteristics of the real 3D flow. For the experiments with the original nozzle, the measured values include the loss in the inlet section, whereas the CFD simulation was applied only to the nozzle inserts. For the 2×20 mm nozzle, the exit area is larger than the cross-sectional area of the inlet duct. This meant a high velocity in the inlet, with correspondingly higher losses there – this accounts for the

Table 5 Comparison of area weighted total gauge pressure ratios ($\bar{p}_{0o,average}/\bar{p}_{0i}$) obtained from CFD and experiment

Nozzle–inlet	Ratio of total pressures from CFD	Ratio of total pressures from experiment	Percentage difference
Plenum-integrated nozzle 1.5×6.3 mm	0.95	0.94	1
Original nozzle with turbine assembly 1.5×6.3 mm	0.66	0.64	3
Original nozzle with turbine assembly 2×20 mm	0.47	0.41	15

slightly greater difference between the experiments and CFD results for this case.

APPENDIX 3 DESIGN AND ANALYSIS OF THE PLENUM CHAMBER AND THE NEW INLET–NOZZLE ASSEMBLY

Owing to the lack of information available in the literature about how to size a plenum chamber, it was necessary to develop analytical and empirical tools to predict the flow characteristics in a plenum chamber. Figure 8 gives an idealized description of the reservoir (which represents the cylinder condition after the pressure regulator) and plenum, in which the important locations are numbered. These numbers are used as subscripts for all variables in the following analysis.

Determination of flow variables: equations and a numerical scheme

It is assumed that the plenum and the nozzle are initially at atmospheric pressure. The equations and the numerical scheme developed below calculate how the
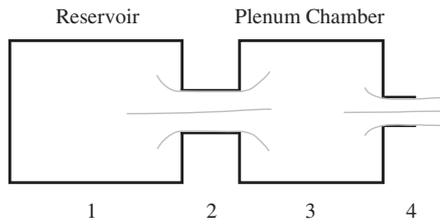
Fig. 8 Schematic diagram of plenum chamber used for unsteady analysis

different flow variables at the numbered locations in Fig. 8 develop with time as the valve in the high pressure cylinder is suddenly switched on. The following computation therefore gives an unsteady analysis, the steady solution is obtained as the asymptotic limit of the same computations.

For isentropic flow, the mass flow through an orifice can be determined if the inlet stagnation pressure, the outlet static pressure, the area of the orifice, and stagnation temperature are known. It is evident that initially when the valve from the cylinder to the plenum chamber is first opened, this is an unsteady problem. The pressure in the plenum chamber would rise because the mass flow at 2 would be larger than the mass flow at 4. Eventually, however, steady state conditions would be reached where the mass flowrate at 2 is equal to the mass flowrate at 4.

Writing the conservation of mass for a compressible fluid

$$\dot{m} = \rho A u \tag{8}$$

The speed of sound in an ideal gas and the equation relating Mach number to velocity can be written as follows

$$a = \sqrt{\gamma R T} \tag{9}$$

$$M = \frac{u}{a} \tag{10}$$

Combining equations (8) to (10) results in

$$\dot{m} = \rho A M \sqrt{\gamma R T} \tag{11}$$

Using the standard relations for isentropic flow [27]

$$\frac{p}{p_0} = \left(\frac{\rho}{\rho_0}\right)^{\gamma} = \left(\frac{T}{T_0}\right)^{\gamma/(\gamma-1)} = \left(1 + \frac{\gamma-1}{2}M^2\right)^{-\gamma/(\gamma-1)} \tag{12}$$

Equation (11) can be written purely in terms of stagnation quantities and pressure

$$\dot{m} = \rho_0 \left(\frac{p}{p_0}\right)^{1/\gamma} A \sqrt{\frac{2\gamma R T_0}{\gamma - 1}\left[1 - \left(\frac{p}{p_0}\right)^{(\gamma-1)/\gamma}\right]} \tag{13}$$

It is a standard practice when formulating numerical schemes to solve for a steady state problem to formulate an unsteady equation where the time derivative represents the level of error present at that time step. This allows the solution to be iterated. Convergence is achieved when the time derivative reaches zero. When the system reaches steady conditions, the mass flowrate at 2 will equal the mass flowrate at 4. This implies that the mass of air inside the plenum chamber (point 3) will not change with time

$$\frac{\mathrm{d}m_3}{\mathrm{d}t} = \dot{m}_2 - \dot{m}_4 = \text{Error in solution} \tag{14}$$

This equation can be represented using a first-order finite difference approximation

$$m_3^n = m_3^{n-1} + \Delta t(\dot{m}_2^{n-1} - \dot{m}_4^{n-1}) \tag{15}$$

where

$$\dot{m}_2 = f\left(\frac{p_3}{p_0}, A_2\right), \quad \dot{m}_4 = f\left(\frac{p_a}{p_0}, A_4\right) \tag{16}$$

Since the cross-sectional area of the plenum chamber is large, it is assumed that the total and static pressure in the plenum chamber are nearly equal. The calculation procedure is as follows.

1. Calculate inlet mass flowrate using p_{01} and p_2.
2. As a simple approximation, assume that the kinetic energy at point 2 is lost as the jet enters into the plenum chamber. As a result $p_2 = p_3 = p_{03}$.
3. Calculate exit mass flowrate using p_{04} and p_4. p_{04} is assumed to be the same as p_{03} which is calculated using equation (12). The plenum Mach number is calculated from equation (11).
4. Calculate the net mass flow out of the plenum chamber and hence the updated mass of fluid inside the plenum chamber.
5. Calculate the updated pressure in the plenum chamber using the equation of state. The temperature is taken to be the temperature at the exit of the inlet duct.
6. Repeat until the mass of fluid in the plenum chamber reaches a steady state.

Equation (15) was iterated using Matlab for a number of different conditions: cylinder absolute pressure and nozzle width were varied.

Figure 9 shows the time evolution of the plenum inlet and exit Mach numbers. It shows that initially the inlet duct is choked and the mass flowrate through
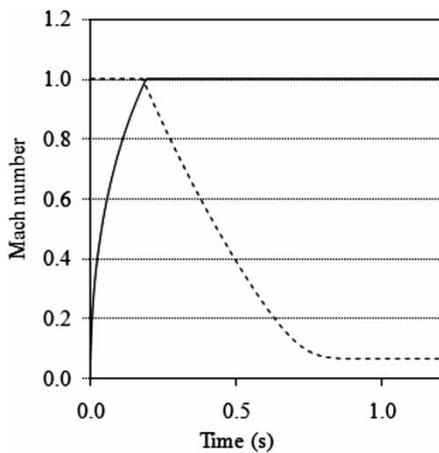
Fig. 9 Development with time of plenum inlet and exit Mach numbers. Keys: - - - - - M_2, ——— M_4 (for an inlet gauge pressure of 3.51 bar)

the exit duct is zero. As time passes, the mass flowrate through the exit duct increases until it reaches choked condition. By this time, the inlet Mach number (M_2) has decreased significantly (since the pressure in the plenum chamber has risen).

This graph shows that it takes up to a second for the plenum chamber to reach steady state conditions. This was taken into account during experimental testing.

Determination of the diameter and length of the plenum chamber

The diameter of the plenum chamber is determined by two methods: (i) simple continuity consideration and (ii) model to include viscous losses.

Continuity consideration

The incompressible continuity equation can be re-arranged to yield the expected plenum velocity for a given diameter ratio

$$u_3 = u_2 \beta^2 \qquad (17)$$

Prediction of total to static pressure ratio including viscous losses

To complement the simple analysis above it was decided to perform an analysis where viscous losses were considered. A flow can be considered stagnant if the ratio of the total pressure to the static pressure is equal to 1. This means that the flow has no bulk-directed kinetic energy. Benedict *et al.* [**32**] performed analysis on sudden enlargements in pipes for steady incompressible flow and provide a means of calculating the change in stagnation pressure and change in static pressure over an abrupt enlargement

$$\frac{p_{03}}{p_{02}} = 1 - (1 - \Phi_2)(1 - 2\beta^2 + \beta^4) \qquad (18)$$

$$\frac{p_3}{p_2} = 1 + 2\beta^2 \left(\frac{1 - \Phi_2}{\Phi_2} \right) (1 - \beta^2) \qquad (19)$$

These two equations can be combined to form a relationship for the total to static pressure after the abrupt enlargement (after flow reattachment has occurred) as a function of the total to static pressure before the abrupt enlargement

$$\Phi_3 = \Phi_2 \left[\frac{1 + 2\beta^2 (1 - \Phi_2/\Phi_2) (1 - \beta^2)}{1 - (1 - \Phi_2)(\beta^2 - 1)^2} \right] \qquad (20)$$

Equation (20) is used to determine an appropriate diameter ratio to produce a near stagnant flow in the plenum chamber, and is plotted in Fig. 10.

Figure 10 shows that, for diameter ratios lower than 0.25, the flow nearly stagnates inside the plenum chamber. As an example, equation (17) predicts the plenum Mach number is 0.019 for an inlet Mach number 0.3 and a diameter ratio of 0.25. Equation (20) would predict a plenum Mach number of 0.02 for these flow conditions. Thus, the two methods give very nearly the same answer.

The other important dimension of the plenum chamber is the axial length. Lau *et al.* [**36**] experimentally showed that for a plenum chamber with a length to diameter ratio of 10 the flow did not completely lose its history as the loss coefficient was still lower than what would be expected from the combined effects of an abrupt enlargement and an abrupt contraction occurring separately. This suggests that the flow still had characteristics of a jet and might not have fully re-attached. The analysis carried out by Benedict *et al.* [**32**] is only valid after the flow has re-attached so it is necessary to find a method to determine the length it takes for the flow to re-attach.

As no analytical tool to make this prediction could be found in the literature it was necessary to use experimental data. So [**39**] carried out a survey of the
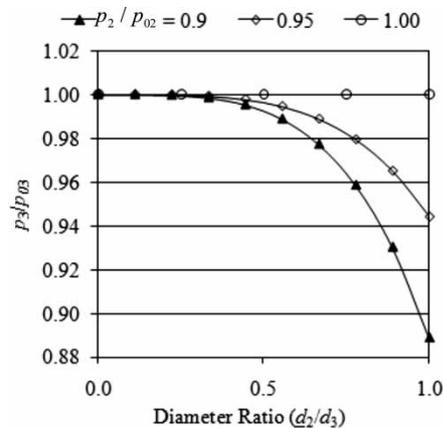
Fig. 10 Ratio of static to total pressure in the plenum with varying diameter ratios (for various p_2/p_{02}, refer to Fig. 8 for locations of points)
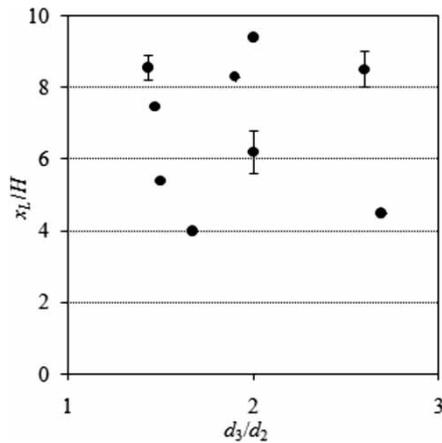
Fig. 11 A plot of x_L/H versus d_3/d_2 for axisymmetric sudden-expansion flows, data from reference [**39**]

literature relating to reattachment lengths for axisymmetric sudden enlargement flows. Figure 11 shows a compilation of the reattachment lengths found by So. The compiled data does not show any systematic pattern for the variation of x_L/H with d_2/d_1. However, this shows that there is approximately a linear relation between the reattachment length x_L and the step height H. The maximum x_L/H value found by So was just under 10.

The following empirical method was used to determine the maximum reattachment length for a chosen diameter ratio

$$H = \frac{(d_2 - d_1)}{2} = \frac{d_1}{2}(\beta^{-1} - 1) \tag{21}$$

It was noted previously that in order to achieve a nearly stagnant condition inside the plenum chamber a diameter ratio of 0.25 was necessary. Equation (21) gives the required value of H as equal to $(3/2)d_1$. Since Fig. 11 shows that the maximum value for x_L/H is 10. Therefore, maximum reattachment length would be $15\,d_1$.

This shows that if the plenum chamber is 15 times the inlet diameter then the flow will reattach. It was decided to design the plenum chamber conservatively so the length was set to 25 times the inlet diameter.